Available online at www.sciencedirect.com
ScienceDirect
Remote Sensing of Environment 107 (2007) 376–384
Remote Sensing of Environment
www.elsevier.com/locate/rse

Using AirMISR data to explore moisture-driven land use–land cover variations at the Howland Forest, Maine — A case study

Lesley-Ann L. Dupigny-Giroux *

University of Vermont, Department of Geography, 200 Old Mill Building, Burlington, VT 05405-0114, USA

Received 27 February 2006; received in revised form 6 July 2006; accepted 4 August 2006

Abstract

Surface moisture stress and vegetation condition can be derived from spectral vegetation indices such as the normalized difference vegetation index (NDVI). The combination of thermal infrared data with these vegetation indices is often plotted as a triangular scatterplot. One such relationship uses the radiant temperatures versus the NIR/blue ratio developed for a semiarid area from Landsat Thematic Mapper data. Given that the thermal range of this index was invalid when applied to a humid temperate region, this study evaluated the utility of using the NIR/blue ratio alone as an indicator of land use/land cover (LULC) separability under spatially varying moisture conditions. It also explored the additional information gained from using multiple view angles (MVA) of this ratio. Results indicate that for the Howland Forest, Maine study site in August 2003, the MVA version of the NIR/blue ratio discriminated among moisture-driven LULC variations, wetland types and moisture stress extent. Separability was best captured by forward view angles and the optimum multi-angular composite was the An/Af/Bf RGB. The multi-angular ratio was sensitive to variations in species type and vigour, water/vegetation proportions and moisture gradients across emergent wetlands. The study extends the original NIR/blue ratio to include wetlands, aquatic vegetation and other temperate LULC types and has the potential to avoid false change detection while contributing to improved mapping and land cover classifications.

Keywords: AirMISR; Multi-view angle; Land use/land cover; Surface moisture; Band ratio; Wetlands

1. Introduction and background

Spectral vegetation indices have been used to describe variations in vegetation condition over space and time. When these indices are combined with transfer models, field data or geomorphological relationships, inferences can be made about the underlying soil properties (Huete, 2004). The combination of thermal infrared and visible data has been used to evaluate surface moisture conditions, vegetation condition and moisture stress. Many of these studies (e.g. Carlson et al., 1995; Gillies et al., 1997; Goward et al., 1985, 2002; Moran et al., 1994; Nemani et al., 1993; Nemani & Running, 1989) focused on the radiant surface temperature (T_s) and normalized difference vegetation index (NDVI) relationship to quantify areally averaged soil moisture conditions (Goward et al., 2002), evapotranspiration in a deciduous forest (Nemani & Running, 1989) and other biophysical relationships.

A scatterplot of this temperature/vegetation index approach or TVX (Goward et al., 2002) is often triangular or trapezoidal in shape if the full range of vegetation fractions and soil moisture conditions were sampled in the data (Sandholt et al., 2002). Such approaches include the Water Deficit Index (WDI) of Moran et al. (1994), the Surface Moisture Index (SMI) of Nemani and Running (1989), the Temperature–Vegetation Dryness Index (TVDI) of Sandholt et al. (2002), the Vegetation Temperature Condition Index of Wan et al. (2004) and the moisture index of Dupigny-Giroux and Lewis (1999). In all cases, the location of a pixel in the temperature/vegetation index space is related to the fractional vegetation cover, evapotranspiration, net radiation, thermal properties of the surface, atmospheric forcing and a series of other inter-related factors. In addition, the intercept and slope of the TVX relationship vary with surface type and could also be a function of the scale at which phenomena were sensed (Sandholt et al., 2002). The

* Tel.: +1 802 656 2156.
E-mail address: ldupigny@uvm.edu.

0034-4257/$ - see front matter © 2006 Elsevier Inc. All rights reserved.
doi:10.1016/j.rse.2006.08.015

TVX approach describes the relative variations in surface moisture conditions, from which absolute soil moisture values can be derived by applying inversion techniques (e.g. Gillies et al., 1997). By factoring in the energy balance principles and quantifying the rate of latent heat flux lost by evapotranspiration, the WDI defines actual water status of a bare soil and mixed vegetation surface (Colaizzi et al., 2003).

The moisture index of Dupigny-Giroux and Lewis (1999) differs from the other reported triangular TVX relationships in its use of the near-infrared/blue ratio to describe vegetation and other land cover characteristics. It was created from Landsat Thematic Mapper (TM) data for the semiarid Brazilian nordeste (northeast) and summarized in Fig. 1. The vertical asymptote at TM 4/1 = 0 represented a water line (clouds, water bodies). The horizontal asymptote at TM 6 = 295 K denoted fully moist conditions, anchored by water bodies and fully vegetated regions. Lines parallel to this asymptote were isomoisture lines along which the LULC type or density varied. The negatively sloping hypotenuse represented a moisture gradient from dry to wet conditions. Movement parallel to and approaching the hypotenuse denoted drying and/or senescence.

With the exception of the summer of drought years (e.g. July 1999), the moisture index was not well validated in a humid, continental mid-latitude climate (Vermont) (Dupigny-Giroux, unpublished results). In this new context, no water line was distinguished and the horizontal asymptote was poorly defined. The triangular spectral space was not observed in cooler seasons (e.g. April 1998). Poor validation was a function of atmospheric forcing and vegetative differences. In particular, the relatively constant incoming solar radiation in the semi-arid context led to small fluctuations in surface temperatures and a thermal range of 295–310 K. In contrast, solar radiation at 45°N varied with solar altitude and time of year, such that the horizontal asymptote equaled 265 K in the spring, 295 K in summer and 288 K in the autumn.

Even more fundamental was the difference in vegetative response to climate, especially precipitation inputs. First, temperate feature types such as wetlands and various types of water bodies were absent in the semi-arid calibration context and therefore, in the spectral space of the original index.

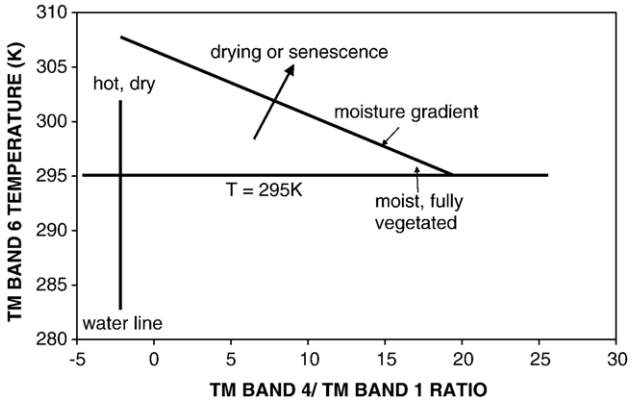

Fig. 1. Triangular temperature/vegetation index given by the Landsat Thematic Mapper 6 surface temperatures vs. TM 4/TM 1 ratio values.

Secondly, in the semi-arid environment, the natural vegetation was adjusted to low moisture inputs with little change in annual biomass amounts. Therefore, the index captured variations in spectral response under drought conditions, even though the actual standing biomass may not have changed. In contrast, in the humid continental regions (i.e. Vermont) where abundant precipitation is the rule, the index responded to the variations in the standing biomass and moisture levels.

The non-validity of thermal ranges across climate regimes raises the question about the applicability of the NIR/blue ratio alone as a mechanism for land use/land cover (LULC) separability. This study proposes to address this question by using data from multiple view angles. Multi-angle imaging or the use of multiple view angles (MVA) of terrestrial ecosystems reveals additional information not observed using spectral data from the nadir or other single view angles, due to the highly anisotropic reflectance of vegetation (Asner et al., 1998). The nadir view angle may not be the most sensitive to vegetation parameters (Privette, 1995). MVA data have fueled further studies of the structure and spatial distribution of vegetation with the sensor's instantaneous field of view (Widlowski et al., 2004; see Diner et al., 2005a for a full description of these studies). The combination of differences in directional reflectance characteristics with multispectral variations has been used in land cover classification and to distinguish among land cover types in a single band at multiple view angles (Hyman & Barnsley, 1997). Zhang et al. (2002a,b) also explored the role of pixel and subpixel heterogeneity as a way of improving existing land cover classifications. The relationship between view angle and reflectance anisotropy at the red wavelengths was found to be a function of the physical properties and geometries of the land surface features (Pinty et al., 2002).

Many MVA studies to date examined biophysical processes such as Leaf Area Index, vegetation structure assessment (Chen et al., 2003; Gobron et al., 2002), NDVI sensitivity to view angle (Goodin et al., 2004) and Bidirectional Reflectance Distribution Function (BDRF) (see Lobell et al., 2002 for a comprehensive list). Some focused on arid and semi-arid environments (Chopping, 2000; Chopping et al., 2003; Lucht et al., 2000; Ni & Li, 2000). Fewer studies addressed surface moisture characteristics. Pinty et al. (2003) used multi-angle imaging to distinguish between surface water which scatters red wavelengths preferentially forward versus dark soils that scatter these wavelengths backwards. Vanderbilt et al. (2002) used the variations in directional signatures among open water, flooded vegetation and non-inundated vegetation to derive a classification technique based on the glitter off a water surface. Abdou et al. (2001) examined the role of antecedent moisture in influencing Airborne Multi-angle Imaging SpectroRadiometer (AirMISR) hemispherical directional reflectance factor (HDRF).

This paper extends the work of Dupigny-Giroux and Lewis (1999) by examining whether additional value can be derived from multi-angle NIR/blue ratios. The specific study objectives were to use one AirMISR flight over the Howland Forest in Maine as a case study:

— to explore the usefulness of the NIR/blue ratio for land use/land cover separability under spatially varying

surface moisture conditions in that humid, continental context;
- to quantify the additional information derived from using multiple view angles of this ratio and to create an optimal multi-angular composite that best highlights feature separability;
- to determine whether wetlands and other moist features could be discriminated from other feature types on this single date, given their absence in the original semi-arid calibration context.

2. Data and methodology

2.1. AirMISR program

From 1997 to 2004, the AirMISR instrument was flown over selected temperate and tropical study areas. Flying at an altitude of 20 km on the NASA ER-2, this pushbroom imager used a single camera on a pivoting gimbal mount to collect data at the nine viewing angles used on the spaceborne MISR instrument. These angles are nadir (An), 26.1° fore (Af) and aft (Aa), 45.6° fore (Bf) and aft (Ba), 60.0° fore (Cf) and aft (Ca) and 70.5° fore (Df) and aft (Da). The swath width of the imagery varied from 11 km at nadir to 32 km for the D cameras. Four spectral bands were centered at 446 nm, 558 nm, 672 nm and 867 nm (blue, green, red and near-infrared) (Diner et al., 1998).

2.2. Study area

The Howland Forest encompasses the towns of Howland and Edinburg, Maine, located southwest of the confluence of the Piscatuquis and Penobscot Rivers, about 56 km (35 miles) north of the city of Bangor, Maine (Fig. 2). Boreal-northern hardwood transitional forest and palustrine wetlands are the dominant land cover type. Forest species include spruce–hemlock–fir, aspen–birch and hemlock–hardwood. The topography is undulating and the elevation decreases towards the east and south, from over 120 m in the north to about 19 m in the south. The Howland Forest is well instrumented with standard meteorological equipment, biomass and carbon sequestration measurements to support long term experiments including NASA's Forest Ecosystem Dynamics Project, an AmeriFlux tower and collaborations among the University of Maine, the Woods Hole Research Center and the U.S. Forest Service (CRESS, 2002).

2.3. AirMISR data for Howland, Maine

On 28 August, 2003 AirMISR data were collected during north–south and east–west flight runs over the study area. On the former run, the geometric product data collection began at 16:20:52 with the Df camera and ended at 16:32:15 with the Da camera, spanning a latitudinal range from 45.0°N to 45.43°N. The solar zenith angle during the north–south run varied from 36.72° in parts of the Df view angle to 36° at the Ca angle. Solar zenith angles on the east–west run spanned 35.46–35.6° over all view angles. For both runs, integer radiances of the level 1 georectified radiance product (L1B2) data were resampled to a 27.5 m grid in the UTM (Universal Transverse Mercator) projection and available online from the Langley Distributed Active Archive Center (DAAC). Actual radiances were computed using the AirMISR tool. An IR minimum check was performed for each viewing angle. For the north–south run, the ozone optical depth was zero, the aerosol optical depth 0.0628 and the Rayleigh optical depth ranged from 0.0153 for the NIR, to 0.227 for the blue wavelengths. With the optical depth values less than 0.3, no further atmospheric correction was applied (AirMISR Howland_2003

Fig. 2. Sketch map of the United States (a) showing the location of the study site (black star) in the state of Maine (b). Maps courtesy of the U.S. Census Bureau.

Quality Summary, 2004). Ancillary digital data were acquired from the Maine GIS and included landforms, surface hydrology, the National Wetlands Inventory, as well as the land cover and wetlands of the Gulf of Maine. The latter dataset is based on NOAA's Coastal Change Analysis Program (C-CAP) Land Cover Classification System.

2.4. NIR/blue ratios and multi-angular compositing

Image processing was performed with the ENVI® software. The NIR/blue ratio was computed for each of the nine viewing angles. Using the nadir view angle of the north–south run, seventy-four regions of interest were delineated (with standard deviations of 0.01–0.27) to include both vegetative and non-vegetative LULC types (water, roads, barren ground). Special attention was paid to the palustrine wetland areas extracted from the National Wetlands Inventory, as well as anomalous regions observed on a false colour infrared (CIR) composite of the scene. ENVI®'s tool called reconcile regions of interest via map was used to "transfer" the 74 regions of interest to the eight remaining view angles. This tool defines the selected regions in overlapping georeferenced images "regardless of differences in image or pixel sizes between the two images" (RSI, 2004). The accuracy of the geolocation was verified spatially. For each viewing angle, the NIR/blue ratio values in the 74 regions were spatially queried and the results used to create comparative scatterplots of every possible pairing of view angles. Best fit lines were computed for each view angle pair. The 74 regions of interest were also reconciled to the north–south elevation data collected as part of the L1B2 data at nadir, from which a scatterplot of the LULC-elevation association was created. Multi-angular RGB colour composites of the ratioed images were created by grouping three viewing angles at a time. The optimal view angle composite was selected on the basis of visual comparison of the multi-angular composites, the best fit regression results and covariance-based Principal Components Analysis (PCA).

3. Results and discussion

Although the above methodology was applied to both flight runs, the results will focus only on the north–south run for a number of reasons. The first is that although ENVI®'s reconcile

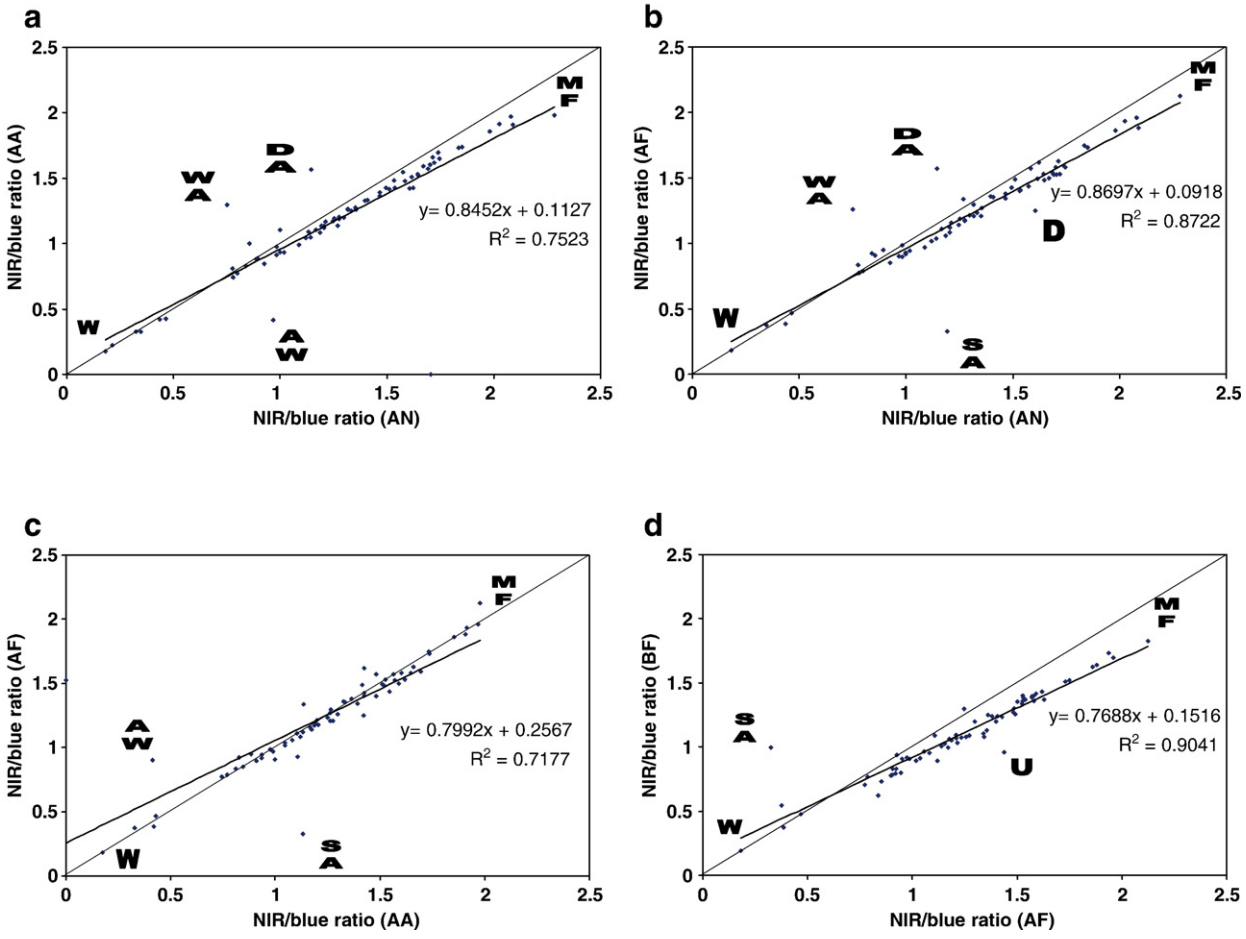

Fig. 3. Comparisons of the NIR/blue ratios for anomalous and other selected features for the Aa and An cameras (a), An vs. Af cameras (b), Aa vs. Af cameras (c) and Af vs. Bf cameras (d). Feature types are water and persistent emergent wetlands (W); water-dominated intertidal emergent and subtidal aquatic vegetation (WA); drying estuarine subtidal aquatic bed (DA); acid, saturated needle-leaf forested wetland (AW); very dry subtidal aquatic bed/intertidal emergent vegetation (MF); dead forested wetland (D); transitional subtidal aquatic and intertidal emergent vegetation (SA); and upland needle-leaved evergreen forested wetland (U). The 45° line, best fit line and regression statistics are also given.

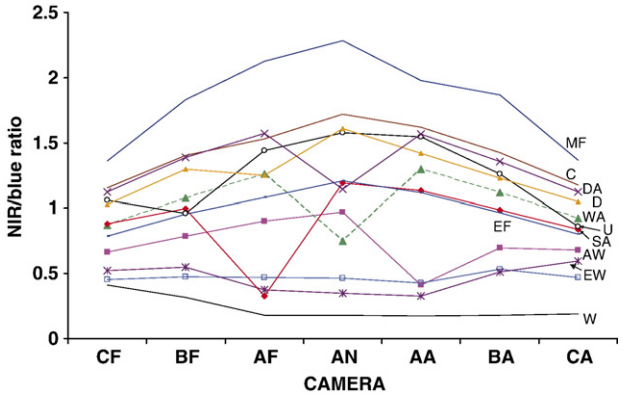

Fig. 4. Variations in NIR/blue ratio as a function of viewing angle for the anomalous and selected features listed in Fig. 3.

regions of interest via map tool was expected to result in similar values between runs, this only held true for the elevation data ±0.2 m. Secondly, a potential hotspot effect at the Af view angle (26.1°) of the east–west run coincided with the maximum NIR/blue ratios for many feature types, hindering their separability. For the north–south run, the viewing angles at ±70.5° were not included in the results due to geometric distortions (skew and tangential symmetric) or aircraft jitter (Diner et al., 2005b). According to the online Quality Summary for this data set (AirMISR Howland_2003 Quality Summary, 2004), geometric errors on the order of 150 m were observed in preprocessing due to insufficient GCPs (ground control points). The summary also noted that striping resulted from large pixel to pixel uncertainties and the stretching of radiometric values.

3.1. Comparison of camera pairs

The relationship among the regions of interest at the An, Af, Aa and Bf view angles is shown on Fig. 3, which also includes the 45° line, best fit line and regression statistics. With the exception of some outliers, the points lie on a straight line and indicate a high degree of correlation between view angles (An, Af, Aa (Fig. 3a–c). The relationship represents a moisture gradient from mesic regions (low values) to xeric ones (high ratios). Deep water bodies, a treatment pond and seasonally flooded persistent, emergent wetlands (Cowardin et al., 1979) were found at the wet end (W). The highest ratios were observed for dry estuarine subtidal aquatic and intertidal emergent vegetation (MF), bare ground, developed areas and cropland. The dry estuarine area displayed an extremely high NIR radiance associated with a concentration of organic material near the surface of the water as draw-down occurred. Other LULC types such as roads, evergreen forests, silty water bodies, scrub–shrub wetlands and forested wetlands were found between the two extremes.

Several anomalous regions were noted. For both the forward and aft angles (Fig. 3a,b), higher NIR/blue ratios were observed in a dry estuarine subtidal aquatic bed (DA), as well as an estuarine intertidal emergent/ subtidal aquatic vegetation region (WA) with a higher water content than other similar regions. These two anomalies highlight that similar displacements are produced by very different processes (Govaerts et al., 1999) — the drying of a wetland that tends to be dominated by plants growing on the surface (DA) versus rising water levels in a salt marsh (WA). The aft camera also highlighted an extensive, low-lying acidic and saturated needle-leaved evergreen forested wetland (AW) with a nadir ratio twice that of the aft angle. At the forward viewing angle (Fig. 3b), an anomalous area of subtidal aquatic and intertidal emergent vegetation (SA) had an opposite change vector compared to the other estuarine habitats (WA and DA). A dry, dead forested wetland (D) was also observed. Plotting the 26.1° fore and aft viewing angles against each other (Fig. 3c) highlighted many of the aforementioned anomalies, with the Af ratio for the saturated, acidic wetland (AW) being twice that of the aft view angle.

The forward viewing angles were sensitive to variations in wetlands and other vegetation with tidal flow regimes. The comparison between the Af and Bf cameras (Fig. 3d) had the best fit line of the four camera pairings (R^2=0.904), but the largest angular departure from the 45°line. Interestingly, the vertical asymptote around Af=0.4 represented both a moisture gradient as well as a shift towards increasingly permanent vegetation species. Seasonally flooded/saturated persistent emergent wetlands were found at the lower end of the asymptote, with the anomalous aquatic and emergent vegetation (SA) at the upper end. The final anomaly was the seasonally flooded, terrene (headwater) needle-leaved evergreen forested wetland (U) located at 117.5 m, one of the highest points on the landscape. Tiner (2003) noted that forested wetlands with seasonally flooded water regimes tend to be wetter for shorter durations in the growing season. Thus, the ability to view them at the 26.1° and 45° angles facilitates the quantification of moisture stress not observable at nadir.

3.2. Comparison of viewing angles

Fig. 4 summarizes the variations in the NIR/blue ratios across view angles for the seven anomalous and four other LULC cover types common at the study site. The moisture gradient across the landscape was again observed with the deep "pure" water bodies (W) having low, almost constant ratios at all angles, and the stressed estuarine aquatic and emergent vegetation (MF) having the highest. The highest NIR/blue ratios for water bodies occurred at the larger forward view angles (Cf and Bf). The peakedness of the MF curve indicates not only the severity of the moisture stress in this saltwater habitat, but also the marked vertical variations in emergent and surface vegetation across the area. Variations among species type, health and moisture content fell between these two extremes of water and stressed estuarine vegetation. Both croplands (C) and evergreen forests (EF) had bell-shaped curves, with the former having higher ratios (1.2–1.5) across all cameras than the latter (less than 1.0).

Bowl-shaped anisotropy was observed for the seasonally-flooded, beaver-impounded persistent emergent wetland (EW). This category of wetlands tends to be predominantly water logged such that the standing water of this particular terrene wetland dominated the near-nadir viewing angles (Af, An, Aa). At the larger view angles, more of the vegetation fraction was

observed resulting in larger ratios (Fig. 4). The crossing of the lines representing two parts of this same wetland suggests that differing amounts of standing water versus vegetation were observed across view angles. Bowl-shaped curves have also been observed in studies of the NDVI (e.g. Goodin et al., 2004) and sensitivity of crown shading (e.g. Asner, 2000). Using red wavelengths to examine the role of directional solar radiation on vegetation, Pinty et al. (2002) observed bell-shaped anisotropy patterns for heterogeneous surfaces and bowl-shaped anisotropy for homogeneous ones.

The remaining features on Fig. 4 were characterised by decreases or darkspots in the NIR/blue ratio at one of the A cameras or the Bf one. The dramatic Af darkspot of the aquatic/emergent vegetation (SA) suggests that although the herbaceous vegetation in this region had become established enough to resemble evergreen forests at most view angles, the strong NIR absorption at the Af angle indicated its residual wetland characteristics. The much smaller Af darkspot for the seasonally flooded dead, evergreen forested wetland (D), only appears as such in juxtaposition with the anomalously high NIR radiances (and ratio) at nadir. The latter is related to the increased albedo observed when needle-leaf vegetation is stressed (Yin, 1998).

The An darkspot belonged to water-dominated LULC types (subtidal (WA) and intertidal regimes (DA)), with more vegetation being present on or below the water surface in the subtidal case. Both areas were located at moderately high elevations (45–50 m) and were lotic (alongside a stream). The intertidal vegetation was found on an island in the middle of a third-order stream, with the NIR/blue ratios being the only indicators of the stress not observed in the original multispectral data or false CIR composites. In contrast, the subtidal aquatic vegetation was found west of a first order stream, with moisture stress approaching that of the driest estuarine feature (MF). This ability to separate aquatic vegetation on the basis of their NIR differences (Gower et al., 1999) is one of the major contributions of this study.

The Aa darkspot was observed for the anomalous acidic, saturated needle-leaved evergreen emergent wetland (AW). Most wetlands of this type had low NIR/blue ratios (0.8–1.0) across all view angles, and could have been mistaken for silty water on the original spectra or false CIR composites. The darkspot for the anomalous wetland could be a function of either more shadows or NIR absorption at the aft view angle. Finally, the Bf darkspot for the seasonally flooded, needle-leaf evergreen wetland (U) may be related to its higher elevation (117.5 m) in relation to viewing geometry, given its overlap with other wetlands and aquatic vegetation at the nadir and aft viewing angles.

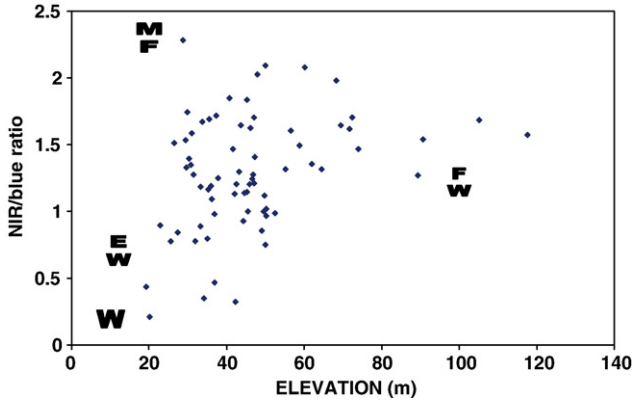

Fig. 5. Variations in NIR/blue ratio as a function of elevation (m) at the An (0°) viewing angle.

Table 1
Principal Components Analysis showing the eigenvalues as a percentage and component loadings for the first five components

	All cameras	Fore and nadir	Aft and nadir
PC1 % explained variance	53.6157	48.30647	71.11616
PC2 % explained variance	18.93087	26.89032	11.64495
PC3 % explained variance	7.66057	11.35003	6.858189
PC4 % explained variance	6.658458	4.160751	3.070382
PC5 % explained variance	2.377662	2.386031	2.349151
PC1 highest loading	Ca red (0.559465)	An red (− 0.809289)	Aa red (0.389072)
PC2 highest loading	Ca green (− 0.660514)	An NIR (− 0.768093)	Ba red (0.398203)
PC3 highest loading	Ca green (0.722172)	An NIR (0.589100)	Ca blue (0.512574)
PC4 highest loading	Af red (− 0.683879)	Cf red (0.589100)	An green (− 0.695356)
PC5 highest loading	Af NIR (0.515433)	Bf red (0.643563)	Ba red (0.527130)

Results include the Cf to Ca (all) cameras; An, Af, Bf and Cf (fore) cameras; An, Aa, Ba and Ca (aft) cameras.

3.3. The NIR/blue ratio and elevation relationship

The relationship between the NIR/ratio and elevation at nadir was weakly logarithmic (Fig. 5). Three subregions were clearly distinguished. At the lowest elevations, features with low ratios included water bodies and persistent emergent wetlands that are seasonally flooded (W). The highest elevations were clustered in the northwestern part of the image and included a variety of seasonally flooded, needle-leaved evergreen forested wetlands (FW) with and without broad-leaved species. It is interesting to note that the upland regions were not the driest parts of the landscape. Similarly, the highest ratio was observed for the stressed estuarine aquatic bed/intertidal emergent wetland (MF) at an elevation (28.8 m) that was more like the persistent emergent wetlands which had among the lowest ratios. This suggests that site-specific variations and stressors were more important factors than elevation alone in determining the NIR/blue ratio of a given feature. The final grouping of interest were the very high NIR/blue ratios (>2) that belonged to bare ground, agriculture and development found over a range of elevations. All other feature types were found between these three groups.

3.4. Optimal angular composite

Principal components analysis was used to examine the structure of the relationships across view angles. It was

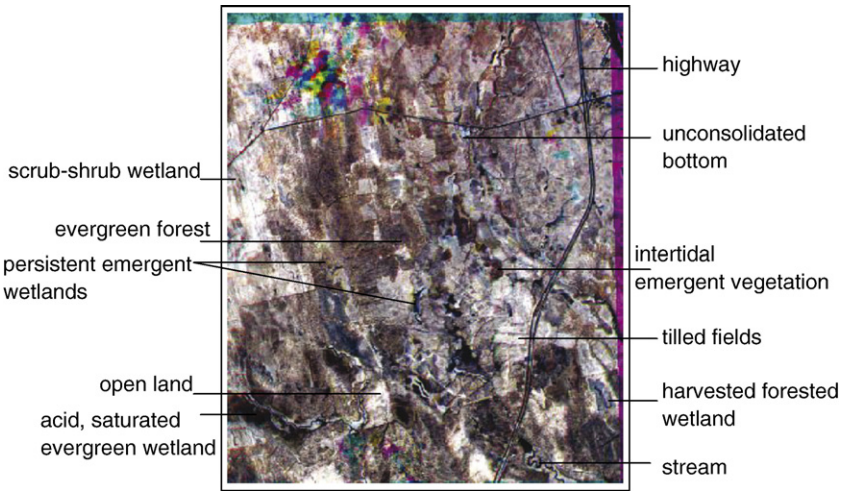

Fig. 6. Optimal multi-angular colour composite using the An(R), Af(G) and Bf (B) cameras.

performed on the four bands at: a) all the viewing angles, b) the forward angles including nadir and c) the aft angles with nadir view (Table 1). Principal component 1 (PC1) of the aft plus nadir view angles accounted for the highest explained variance (71.1%) while the fore plus nadir angles had the lowest (48.3%). This implies that the aft view angles were highly correlated, while the fore angles were very dissimilar. PC2 is usually a change or atypical component and the large percent explained variance for the fore/nadir angles (≈ 27%) again suggests dissimilarities. The first five components of the fore angles were dominated by NIR and red wavelengths at nadir, Cf and Bf view angles, with very weak correlations in the remaining loadings (Table 1). Negative loadings at the Bf NIR and blue (An blue) wavelengths were observed for the first three (two) components.

These results highlight that the blue and near-infrared wavelengths of the nadir, Af and Bf cameras capture maximum variations across the landscape. The best fit regression lines were for the Af–An and Af–Bf relationships (R^2 of 0.87 and 0.904 respectively) (Fig. 3). Thus, the optimal multi-angular composite was given by the An(R), Af(G) and Bf(B) angles (Fig. 6). Major roads and water courses appear black, as do acid, saturated evergreen wetlands and some persistent emergent wetlands. Areas of intertidal emergent vegetation are primarily dark brown, while shades of blue denote subtidal aquatic vegetation. Regions in both intertidal and subtidal flow regimes appear as bright blue. Evergreen forests are rough textured shades of mauve. Open land regions are white and can be distinguished from tilled fields by the subtle rows of the latter.

4. Summary and conclusions

The results highlight that on this date in August 2003, the NIR/blue ratio at multiple view angles successfully discriminated among LULC types of spatially varying surface moisture characteristics in a transitional, forested region of central Maine. Variations among wetland types and moisture stress extent were also distinguished. Lowest NIR/blue ratios at all angles denoted water bodies, while water-dominated wetlands with low vegetation contents had bowl-shaped anisotropy with slightly higher ratios (Fig. 3). Bell-shaped anisotropy was observed for crops, deciduous and evergreen forests. Very large NIR/blue ratios were associated with dry, estuarine vegetation, open land and moisture stress in certain wetlands. Darkspots at the Af view angle were related to moisture stress in palustrine forested wetlands. The Bf darkspot corresponded to an upland needle-leaf forested wetland, while the Aa one was related to shadowing or NIR absorption in an acidic, forested wetland. A scatterplot of the Af and Bf ratios revealed a vertical asymptote at Af=0.4, which represented a moisture gradient and shift towards increasingly permanent vegetation.

Three main factors contributed to the success of the multi-angular NIR/blue ratio in this case study. The first was the higher spectral resolution of the AirMISR bands compared to the original TM ones. Secondly, the use of multiple view angles allowed for feature separability on the basis of phenology and moisture characteristics. In particular, this multi-angle viewing of wetlands expands the recommended use of the 15–30° solar illumination angle with the nadir viewing angle for optimally recording benthic features (Dobson et al., 1995). The multi-angular ratio was sensitive to variations in species type and vigour, water/vegetation proportions and moisture gradients across emergent wetlands. The spectral response of aquatic plants varies with environmental factors such as water temperature, salinity and the movement of water around the plants (Fyfe, 2003). In the An and Af spectral space, the difference in change vectors for the anomalous areas of the drying aquatic vegetation, a dead forested wetland and an upland evergreen wetland indicates the influence of very different types of stressors. Other studies (e.g. Anderson et al., 2004) have also noted that stress or unusual growing conditions can be extracted from outliers in vegetation indices based on NIR and red reflectances. These variations in moisture stress among aquatic vegetation, crops, evergreen forests and forested wetlands would not have been possible at a single view angle (Lobell et al., 2002). This ability to quantify stress across the landscape helps to fill in a knowledge gap noted by Asner (2000). Fyfe (2003) suggested that the blue and NIR wavebands be used to discriminate seagrasses in southeastern Australia because of the

poor species separation at the blue wavelengths and the distinction of plant material floating on water surfaces in the NIR. The Maine study shows that the NIR/blue ratio also distinguished between aquatic macrophytes and terrestrial vegetation which are often similar in single wavebands (Valta-Hulkkonen et al., 2003).

The third major factor in the success of the multi-angular ratio were the antecedent moisture conditions. At the macro level across Maine, the spring and summer of 2003 were respectively the fifth and eighth driest on record since 1895. Longer term dry conditions extended back to 1998 with five of the eight driest summers on record falling in the 1999–2003 time frame. At the temporal finer scale, although precipitation at Bangor, Maine was close to the climatological average during May and June, 2003, only 22.6 mm fell in July and 50 mm in August, compared to averages of 82.3 mm and 75.56 mm respectively. No rain fell during the 13 days prior to the AirMISR data acquisition. These short and longer term moisture deficits likely affected the phenology of the vegetation, as well as the vegetation/water proportion in systems that are flooded/saturated on varying time frames. Xiao et al. (2004) noted that photosynthetic activity in evergreen needleleaf forest at the Howland research site peaks in July. Drought can accelerate the phenology in this environment (Dupigny-Giroux, 2001) and if this acceleration occurred in conjunction with moisture deficits, this could account for the anomalously high NIR radiances observed for some features (Jensen, 1986). More importantly, the moisture-stressed landscape was a closer approximation to the dry conditions under which the original form of the moisture index was calibrated.

In extending the original NIR/blue ratio to include wetlands, aquatic vegetation and other mid-latitude LULC types, the multi-angular ratio has the potential to contribute to improved mapping and land cover classification (Barnsley et al., 1997; Bicheron et al., 1997) in humid, temperate regions. The ability of the NIR/blue ratio to separate wetlands could assist in avoiding false change detection due to drought or water drawdown (U.S. Fish & Wildlife Service, 2004) at these latitudes. It could also be helpful in the photointerpretation of evergreen forested wetlands and more xeric ecosystems, which to date, have been difficult to monitor (Tiner, 2003).

In the future, the multi-angular ratio should be validated over areas of greater homogeneity (as opposed to a transitional forest) and for an extended time series of data to quantify sources of error due to subpixel heterogeneity. The ratio should also be compared with higher spatial and spectral resolution data (e.g. AVIRIS) and/or used in conjunction with field data to quantify the role of vegetation density, height and shadowing on subpixel surface heterogeneity. Finally, the methods should be applied to coincident MISR data to test their applicability across scales in the same way that the original moisture index was found to be scalable from Landsat Thematic Mapper to NOAA AVHRR data.

Acknowledgments

The author gratefully acknowledges the Jet Propulsion Laboratory's David J. Diner for his technical advice and Linda Hunt for creating the AirMISR import script for ENVI. Also acknowledged are the NASA Langley ASDC DAAC and RSI Inc. for their invaluable assistance with the data import and suggestions. Alan Howard of the University of Vermont provided statistical advice. These data were obtained from the NASA Langley Research Center Atmospheric Sciences Data Center. This manuscript was strengthened by thoughtful reviews from Ruth Defries and three anonymous reviewers.

References

Abdou, W. A., Conel, J. E., Pilorz, S. H, Helmlinger, M. C., Bruegge, C. J., Gaitley, B. J., et al. (2001). Vicarious calibration. A reflectance-based experiment with AirMISR. *Remote Sensing of Environment*, *77*, 338–353.

AirMISR HOWLAND 2003 Quality Summary (2004, February 12). http://eosweb.larc.nasa.gov/PRODOCS/airmisr/HOWLAND_2003/Quality_Summaries/airmisr_howland_2003.html created.

Anderson, M. C., Neale, C. M. U., Li, F., Norman, J. M., Kustas, W. P., Jayanthi, H., et al. (2004). Upscaling ground observations of vegetation water content, canopy height, and leaf area index during SMEX02 using aircraft and Landsat imagery. *Remote Sensing of Environment*, *92*, 447–464.

Asner, G. P. (2000). Contributions of multi-view angle remote sensing to land-surface and biogeochemical research. *Remote Sensing Reviews*, *00*, 1–26.

Asner, G. P., Braswell, B. H., Schmil, D. S., & Wessman, C. A. (1998). Ecological Research Needs from Multiangle Remote Sensing Data. *Remote Sensing of Environment*, *63*(2), 155–165.

Barnsley, M. J., Allison, D., & Lewis, P. (1997). On the information content of multiple view angle (MVA) images. *International Journal of Remote Sensing*, *18*, 1937–1960.

Bicheron, P., Leroy, M., Hautecouer, O., & Breon, F. M. (1997). Enhanced discrimination of boreal forest covers with directional reflectances from the airborne polarization and directionality of Earth reflectances (POLDER) instrument. *Journal of Geophysical Research*, *102*(29), 517–528.

Carlson, T. N, Gillies, R. R., & Schmugge, T. J. (1995). An interpretation of methodologies for indirect measurement of soil water content. *Agricultural and Forest Meteorology*, *77*, 191–205.

Chen, J. M., Liu, J., Leblanc, S. G., Lacaze, R., & Roujean, J. -L. (2003). Multi-angular optical remote sensing for assessing vegetation structure and carbon absorption. *Remote Sensing of Environment*, *84*, 516–525.

Chopping, M. J. (2000). Large-scale BRDF retrieval over New Mexico with a multiangular NOAA AVHRR dataset. *Remote Sensing of Environment*, *74*, 163–191.

Chopping, M. J., Rango, A., Havstad, K. M., Schiebe, F. R., Ritchie, J. C., Schmugge, T. J., et al. (2003). Canopy attributes of desert grassland and transition communities derived from multiangular airborne imagery. *Remote Sensing of Environment*, *85*, 339–354.

Colaizzi, P. D., Barnes, E. M., Clarke, T. R., Choi, C. Y., Waller, P. M., Haberland, J., et al. (2003). Water stress detection under high frequency sprinkler irrigation with water deficit index. *Journal of Irrigation and Drainage Engineering*, *129*(1), 36–43.

Cowardin, L. M., Carter, V., Golet, F. C., & LaRoe, E. T. (1979). *Classification of wetlands and deepwater habitats of the United States.* Washington, DC: U.S. Fish and Wildlife Service FWS/OBS-79-31.

CRESS (2002, February). *CRESS Project: Site#8, Howland.* http://www.geog.umd.edu/cress/s8rep.htm, last updated.

Diner, D. J., Barge, L. M., Bruegge, C. J., Chrien, T. G., Conel, J. E., Eastwood, M. L., et al. (1998). The Airborne Multi-angle Imaging SpectroRadiometer (AirMISR): Instrument description and first results. *IEEE Transactions on Geoscience and Remote Sensing*, *36*(4), 1339–1349.

Diner, D. J., Braswell, B. H., Davies, R., Gobron, N., Hu, J., Jin, Y., et al. (2005). The value of multiangle measurements for retrieving structurally and radiatively consistent properties of clouds, aerosols and surfaces. *Remote Sensing of Environment*, *97*, 495–518.

Diner, D. J., Martonchik, J. V., Kahn, R. A., Pinty, B. A., Gobron, N., Nelson, D. L., et al. (2005). Using angular and spectral shape similarity constraints to improve MISR aerosol and surface retrievals over land. *Remote Sensing of Environment*, *94*, 155–171.

Dobson, J. E., Bright, E. A., Ferguson, R. L., Field, D. W., Wood, L. L., Haddad, K. D., et al. (1995). *NOAA Coastal Change Analysis Program (C-CAP): Guidance for Regional Implementation.* NOAA Technical Report NMFS 123 : Department of Commerce.

Dupigny-Giroux, L. -A. (2001). Towards characterizing and planning for drought in Vermont. Part I. A climatological perspective. *Journal of the American Water Resources Association*, *37*(3), 505−525.

Dupigny-Giroux, L-A., & Lewis, J. E. (1999). A moisture index for surface characterization over a semiarid area. *Photogrammetric Engineering and Remote Sensing*, *65*(8), 937−945.

Fyfe, S. K. (2003). Spatial and temporal variation in spectral reflectance: Are seagrasses spectrally distinct? *Limnology and Oceanography*, *48*(1), 464−479.

Gillies, R. R., Carlson, T. N., Cui, J., Kustas, W. P., & Humes, K. S. (1997). A verification of the 'triangle' method for obtaining surface soil water content and energy fluxes from remote measurements of the Normalized Difference Vegetation Index (NDVI) and surface radiant temperature. *International Journal of Remote Sensing*, *18*(15), 3145−3165.

Gobron, N., Pinty, B., Verstraete, M. M., Widlowski, J. L., & Diner, D. J. (2002). Uniqueness of multiangular measurement — Part II: Joint retrieval of vegetation structure and photosynthetic activity from MISR. *IEEE Transactions on Geoscience and Remote Sensing*, *40*(7), 1574−1592.

Goodin, D. G., Gao, J., & Henebry, G. M. (2004). The effect of solar illumination angle and sensor view angle on observed patterns of spatial structure of tallgrass prairie. *IEEE Transactions on Geoscience and Remote Sensing*, *42*(1), 154−165.

Govaerts, Y. M., Verstraete, M. M., Pinty, B., & Gobron, N. (1999). Designing optimal spectral indices: A feasibility and proof of concept study. *International Journal of Remote Sensing*, *20*(9), 1853−1873.

Goward, S. N., Cruickshanks, G. C., & Hope, A. S. (1985). Observed relation between thermal emissions and reflected spectral reflectance from a complex vegetated landscape. *Remote Sensing of Environment*, *18*, 137−146.

Goward, S. N., Xue, Y., & Czajkowski, K. P. (2002). Evaluating land surface moisture conditions from remotely sensed temperature/vegetation index measurements: An exploration with the simplified simple biosphere model. *Remote Sensing of Environment*, *79*, 225−242.

Gower, J. F. R., Doerffer, R., & Borstad, G. A. (1999). Interpretation of the 685 nm peak in water-leaving radiance spectra in terms of fluorescence, absorption and scattering, and its observation by MERIS. *International Journal of Remote Sensing*, *20*(9), 1771−1786.

Huete, A. (2004). Remote Sensing of Soils and Soil Processes. In S. Ustin (Ed.), *Remote Sensing for Natural Resources Management and Environmental Monitoring: Manual of Remote Sensing, 3rd edition* (pp. 3−52). : John Wiley and Sons, Inc.

Hyman, A. H., & Barnsley, M. J. (1997). On the potential land cover mapping from multiple-view-angle (MVA) remotely-sensed images. *International Journal of Remote Sensing*, *18*(11), 2471−2475.

Jensen, J. R. (1986). *Introductory digital image processing — A remote sensing perspective.* Upper Saddle River, New Jersey: Prentice Hall.

Lobell, D. B., Asner, G. P., Law, B. E., & Treuhaft, R. N. (2002). View angle effects on canopy reflectance and spectral mixture analysis of coniferous forests using AVIRIS. *International Journal of Remote Sensing*, *23*(11), 2247−2262.

Lucht, W., Hyman, A. H., Strahler, A. H., Barnsley, M. J., Hobson, P., & Muller, J-P. (2000). A comparison of satellite-derived spectral albedos to ground-based broadband albedo measurements modeled to satellite spatial scale for a semidesert landscape. *Remote Sensing of Environment*, *74*, 85−98.

Moran, M. S., Clarke, T. R., Inoue, Y., & Vidal, A. (1994). Estimating crop water deficit using the relation between surface–air temperature and spectral vegetation index. *Remote Sensing of Environment*, *49*, 246−263.

Nemani, R. R., Pierce, L. L., & Running, S. W. (1993). Developing satellite-derived estimates of surface moisture status. *Journal of Applied Meteorology*, *32*, 548−557.

Nemani, R. R., & Running, S. W. (1989). Estimation of regional surface resistance to evapotranspiration from NDVI and Thermal-IR AVHRR Data. *Journal of Applied Meteorology*, *28*(4), 276−284.

Ni, W., & Li, X. (2000). A coupled vegetation-soil bidirectional reflectance model for a semiarid landscape. *Remote Sensing of Environment*, *74*, 113−124.

Pinty, B., Gobron, N., Verstraete, M. M., Mélin, F., Widlowski, J. -L., Govaerts, Y., et al. (2003). Observing earthquake-related dewatering using MISR/Terra satellite data. *EOS, Transactions, American Geophysical Union*, *84*(5), 37−43.

Pinty, B., Widlowski, J. -L., Gobron, N., Verstraete, M. M., & Diner, D. J. (2002). Uniqueness of multiangular measurement — Part I: An indicator of subpixel surface heterogeneity from MISR. *IEEE Transactions on Geoscience and Remote Sensing*, *40*(7), 1561−1573.

Privette, J. L. (1995). *Uses of a bidirectional reflectance model with satellite remote sensing data.* Elements of Change 1995, Session I : AGCI.

RSI (2004). *Research Systems Inc., Boulder, Colorado.*

Sandholt, I., Rasmussen, K., & Andersen, J. (2002). A simple interpretation of the surface temperature/vegetation index space for assessment of surface moisture status. *Remote Sensing of Environment*, *79*, 213−224.

Tiner, R. W. (2003). Correlating enhanced national wetlands inventory data with wetland functions for watershed assessments: A rationale for Northeastern U.S. wetlands. *U.S. Fish and Wildlife Service, National Wetlands Inventory Program, Region 5, Hadley, MA* 26 pp.

U.S. Fish and Wildlife Service (2004). *Technical procedures for wetlands status and trends, operational version, Arlington, VA.*

Valta-Hulkkonen, K., Pellikka, P., Tanskanen, H., Ustinov, A., & Sandman, O. (2003). Digital false colour aerial photographs for discrimination of aquatic macrophyte species. *Aquatic Botany*, *75*, 71−88.

Vanderbilt, V. C., Perry, G. L., Livingston, G. P., Ustin, S. L., Diaz Barrios, M. C., Bréon, F. -M., et al. (2002). Innundation discriminated using sun glint. *IEEE Transactions on Geoscience and Remote Sensing*, *40*(6), 1279−1287.

Wan, Z., Wang, P., & Li, X. (2004). Using MODIS land surface temperature and normalized difference vegetation index products for monitoring drought in the southern Great Plains USA. *International Journal of Remote Sensing*, *25* (1), 61−72.

Widlowski, J. -L., Pinty, B., Gobron, N., Verstraete, M. M., Diner, D. J., & Davis, A. B. (2004). Canopy structure parameters derived from multi-angular remote sensing data for terrestrial carbon studies. *Climate Change*, *67*, 403−415.

Xiao, X., Hollinger, D., Aber, J., Goltz, M., Davidson, E. A., Zhang, Q., et al. (2004). Satellite-based modeling of gross primary production in an evergreen needleleaf forest. *Remote Sensing of Environment*, *89*, 519−534.

Yin, X. (1998). The albedo of vegetated land surfaces: Systems analysis and mathematical modeling. *Theoretical and Applied Climatology*, *60*, 121−140.

Zhang, Y., Tian, Y., Myneni, R. B., Knyazikhin, Y., & Woodcock, C. E. (2002). Assessing the information content of multiangle satellite data for mapping biomes. I. Statistical analysis. *Remote Sensing of Environment*, *80*, 418−434.

Zhang, Y., Shabanov, N., Knyazikhin, Y., & Myneni, R. B. (2002). Assessing the information content of multiangle satellite data for mapping biomes. II. Theory. *Remote Sensing of Environment*, *80*, 435−446.